Microfabrication and cold testing of copper circuits for a 50 Watt, 220 GHz traveling wave tube

Colin D. Joye*[a], Alan M. Cook[a], Jeffrey P. Calame[a], David K. Abe[a], Alexander N. Vlasov[a], Igor A. Chernyavskiy[a], Khanh T. Nguyen[b], Edward L. Wright[b]
[a]U. S. Naval Research Laboratory, 4555 Overlook Ave, SW, Washington, DC, USA 20375; [b]Beam-Wave Research, Inc., Bethesda, MD, USA 20814

ABSTRACT

We present the microfabrication and cold test measurement results of serpentine waveguide amplifier circuits at 220 GHz. The circuits were fabricated using a novel embedded polymer monofilament technique combined with Ultraviolet-LIGA to simultaneously create both the beam tunnel and interaction circuits. We find remarkable characteristic matches between the measurements of the best circuits, illustrating that the process developed is able to create repeatable, highly precise circuits with high yield. It was found that slight beam tunnel misalignment can cause very strong stopbands to appear in the operating band due to bi- or quasi-periodicity. The NRL code TESLA-SW/FW has been used to rapidly simulate the as-built structure under a variety of conditions to accurately predict the performance with an electron beam. The tolerances needed on beam tunnel alignment are studied, with implications extending to the THz range.

Keywords: Slow-wave circuit; traveling wave tube; millimeter wave amplifiers; ultraviolet photolithography

1. INTRODUCTION

As vacuum electron devices (VEDs) push up in operating frequency toward the THz range, fabrication tolerances becoming increasingly critical [1]. In particular, the upper millimeter-wave (mmW) and sub-mmW devices require fabrication techniques beyond what have been traditionally associated with VEDs and other components operating in these frequency ranges. One process that is bridging the technology gap between the realm of CNC machining to that of micro- and nano-scale IC fabrication is the LIGA process (from the German acronym for lithography, electroforming and molding). Of particular interest is ultraviolet (UV) LIGA using such photoresists as SU-8 [2, 3], which is a low-cost alternative to high-quality but extremely expensive X-ray LIGA work [4]. Other UV-LIGA work for VEDs includes the use of the KMPR photoresist [5], and silicon DRIE-fabricated oscillators and amplifiers at 220 GHz and 670 GHz [6-8].

A familiar problem in many types of closed-circuit VEDs is the need for a hollow channel, called a beam tunnel, running through the circuit to allow the electromagnetic fields to interact with the electron beam. For wide bandwidth, high coupling, and resistance to oscillation, this beam tunnel should be closely matched to the size and shape of the electron beam. Techniques for creating beam tunnels below 1 mm in diameter have typically been limited to drilling, plunge electrical discharge machining (EDM), or machining in two halves, but these methods have tolerance issues and aspect ratio limitations in the sub-mmW range. Using a novel, Patent-pending embedded polymer monofilament UV-LIGA process [9,10], both the geometrically round beam tunnel and the circuit can be simultaneously created. This method takes advantage of the highly precise optical techniques while simultaneously reducing cost and increasing yield.

Fig. 1 shows a final serpentine waveguide traveling wave tube (SW-TWT) amplifier circuit as fabricated using the embedded polymer UV-LIGA technique. Exceptional precision is evident for this 8:1 vertical aspect ratio structure in parts (a) and (b) of Fig. 1, prior to having brazed on a flat cover. In Fig. 1(d), the beam tunnel entrance is shown with a geometrically round profile. In Fig. 1(e), the final WR3-like input waveguide is shown after the flat cover has been brazed on.

*colin.joye@nrl.navy.mil; phone 202-404-4510; fax 202-767-1280. This work was supported by DARPA and by the U.S. Office of Naval Research.

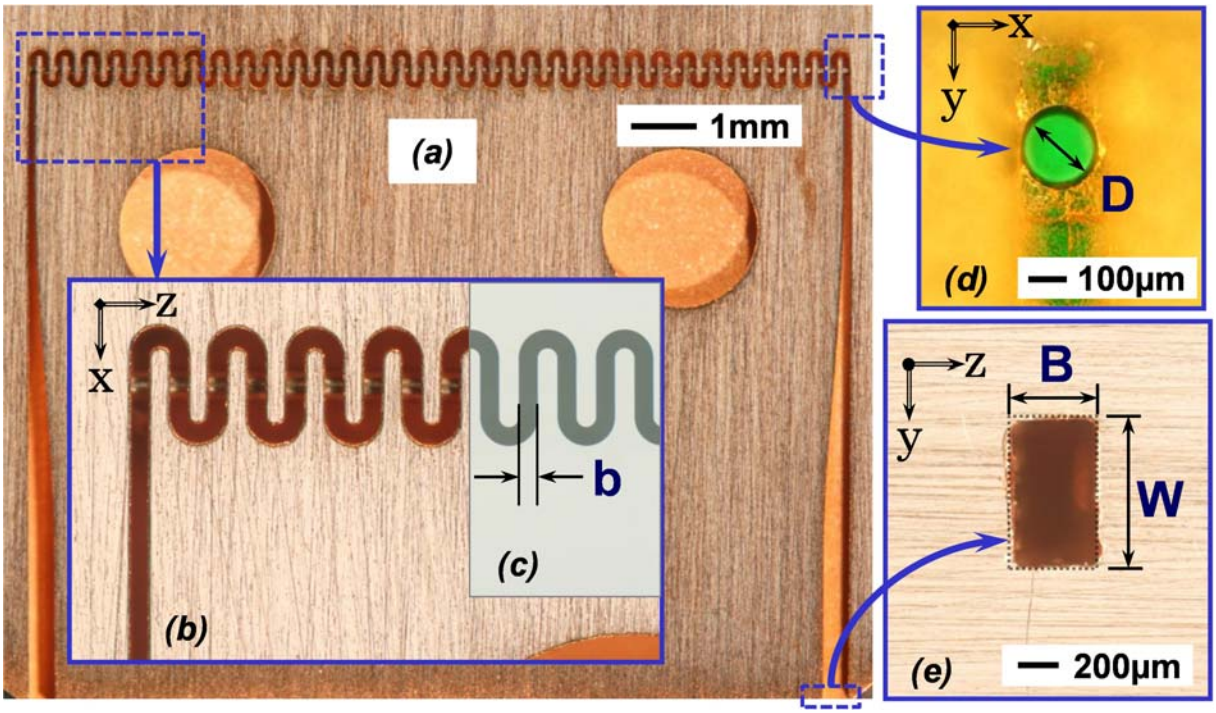

Figure 1. (a) Photo of serpentine waveguide circuit with beam tunnel prior to brazing on a flat cover. Shown with 0.0072 inch diameter gage pin inserted through beam tunnel. (b) Zoom in view of circuit with the gage pin shown inserted, (c) view of the ideal mask pattern, (d) view of beam tunnel on completed circuit, (e) view of input waveguide in completed circuit after brazing.

2. EMBEDDED POLYMER MICROFABRICATION

The key to succeeding with difficult tolerance constraints was the use of an NRL-invented, Patent-pending embedded polymer monofilament UV-LIGA process, described in detail in Ref. [9]. Initially, a lot of attention was given to forming the complete structure in a single UV-LIGA step, which proved to be extremely difficult due to the relatively shallow absorption depth of 300-400 microns in SU-8 photoresist when activated by near-UV at 365 nm. While SU-8 structures up to 600 microns thick were routinely capable of very high tolerance, the yield was extremely poor for single-layer structures of SU-8 over 800 microns thick, due in part to the need for a nearly 9:1 vertical aspect ratio (including extra thickness for polishing later). Fig. 2 shows the highlights of the all-copper two-layer fabrication process that was easily able to overcome these barriers. In Fig. 2(a), the first layer of the structure consists of the SU-8 pattern for a portion of the electromagnetic circuit only, which is then electroformed with copper, and finally lapped to the desired thickness without removing the SU-8. In Fig. 2(b), a polymer monofilament holds the exact size, shape and location of the electron beam tunnel. The polymer material is transparent to UV with a similar index of refraction to SU-8 and is carefully aligned and positioned on the first layer. Next, the SU-8 is applied and exposed as with the first layer. Since the UV passes through the polymer monofilament, it is able to activate SU-8 under the filament and hence form the SU-8 mold as if the filament was not there at all. The copper electroforms around the filament and results in a highly accurate, geometrically round beam tunnel to provide an ideal match to the shape of the electron beam.

3. DESIGN OF AN 11.7 KV TWT

The traveling wave amplifier circuit is designed to make use of available spare parts left over from a 5 W, 218.4 GHz Extended Interaction Klystron (EIK) by CPI, Inc., Model VKY2444 [11]. The serpentine waveguide circuit topology was chosen owing to its compatibility with planar UV-LIGA processes. The circuit was initially designed using MAGIC 3D to maximize the gain and bandwidth from the available space constraints and operating parameters listed in Table 1, which compares the ideal dimensions to the as-built dimensions. The electron beam tunnel was very well aligned in the

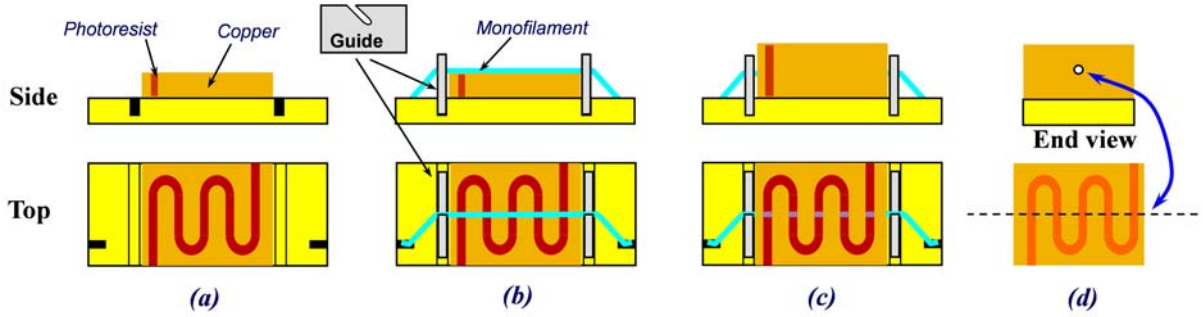

Figure 2. The two-layer embedded polymer monofilament method. (a) The first layer of the circuit is produced by UV-LIGA with the photoresist left behind in the electroformed copper, which is ground and polished to the desired thickness, (b) the monofilament is fixed in place over the first layer, (c) the UV-LIGA process is performed again to create a second layer on top of the first with the monofilament buried inside, (d) dicing to size and the removal of the monofilament and photoresist completes the structure. Beam tunnel location shown by dotted line.

plane of the serpentine bends, being only 3-8 μm out of alignment (3% to 8% of the beam tunnel radius). In the y-direction (Fig. 1), however, the tunnel was off-center by almost a full beam tunnel radius. The effects of this out-of-plane beam tunnel offset are minimal, resulting in slight loss of gain and a shift in center frequency (Fig. 3), while the effect of an in-plane offset or tilt of the beam tunnel gives rise to severe stopbands (Fig. 5), which lead to oscillations.

To mitigate the need for lengthy simulations in PIC-type codes and to accurately determine the performance of the as-built device, the 2.5D large signal NRL code TESLA-CC [12] was extended recently for modeling of TWTs with serpentine (SW) and folded waveguide (FW) circuits [13,14]. The dimensions of the fabricated SW structure have been measured with high precision and have been used as input data for simulations. ANALYST [15] has been used for calculations of dispersion properties and coupling impedances of the fabricated structures. Many details of the fabricated structure have been taken into account for simulations, namely, the actual profile of the waveguide cross section, the actual position of the center of the beam tunnel, and the actual radius of the beam tunnel. The properties of the electron beam have been calculated by the electron code MICHELLE [16] to include a realistic distribution of the focusing magnetic field and a realistic cathode temperature.

The results of electromagnetic simulations of the dispersion properties of the as-built structure are presented in Fig. 3(a) for two cases: When the beam tunnel is perfectly aligned (symmetric case) and when the actual measured dimensions are used (offset). Small variations in the dispersion curves for the same two cases lead to moderate variations of TWT gain in the small signal regime as presented in Fig. 3(b).

Table 1. TWT Design Parameters

Parameter	Sym.	Target	As Fab'd
Period	p	205 μm	205 μm
WG narrow wall	b	105 μm	105 μm ± 5
WG broad wall	W	785 μm	785 μm ± 3
Number of gaps	N	64	64
Beam tunnel diam	D	190 μm	183 μm ± 4
Beam diameter	d	<185 μm	-
Beam voltage	V_0	11.7 kV	-
Beam current	I_0	105 mA	-
Small sig. gain	-	14 dB	-
3 dB Bandwidth	-	15 GHz	-
Max power out	-	>50 W	-
In & out W/G dim.	B	432 μm	428 μm ± 6

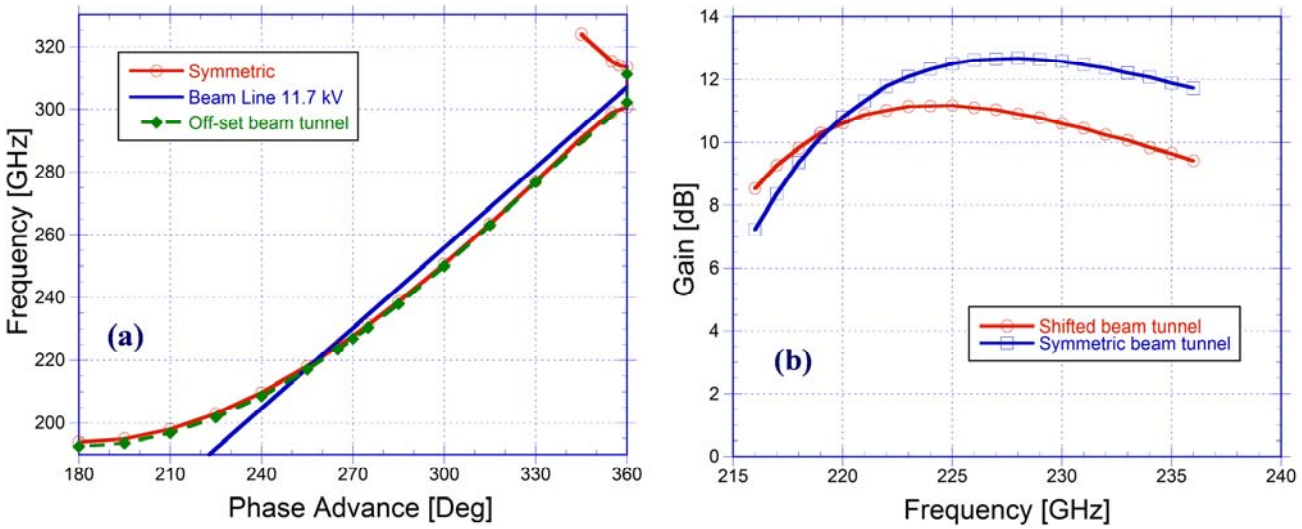

Figure 3. (a) Plot of the dispersion relation for circuit #36LA comparing the ideal symmetric case to the as-built case with the beam tunnel offset from the center plane simulated in ANALYST with high resolution (300,000 finite elements per period). (b) The predicted effect of the offset beam tunnel in the small signal regime using TESLA-SW/FW.

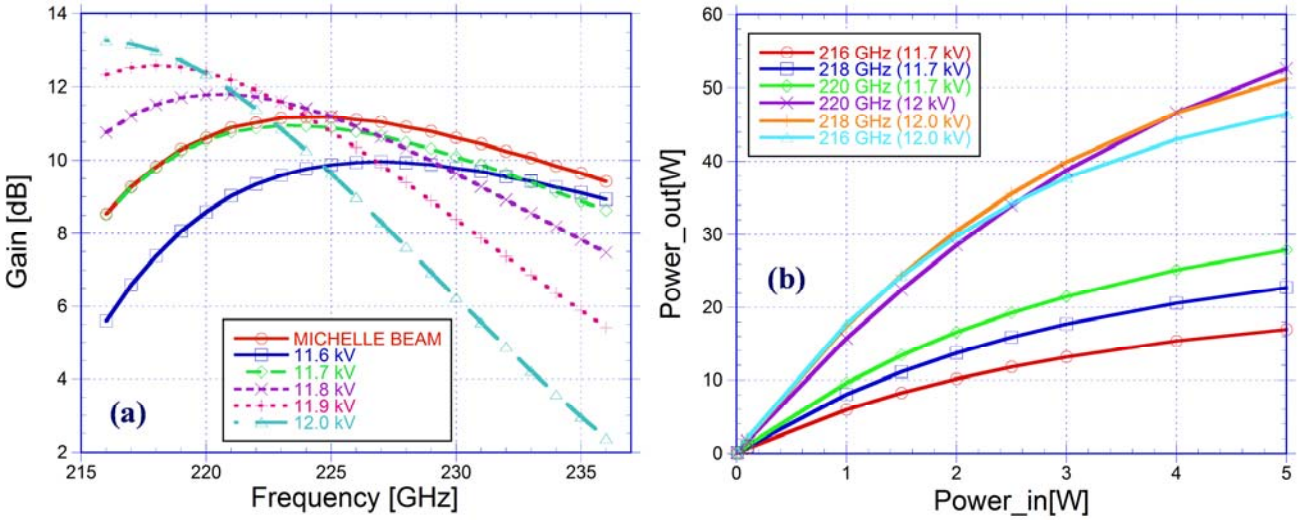

Figure 4**.** Predicted performance of the as-built SW-TWT amplifier at various operating parameters using TESLA-SW/FW. (a) Predicted small-signal gain at various voltages. All simulations were performed using a cold electron beam, except for one that used a thermal beam from the beam optics code MICHELLE. (b) Predicted drive curves at three frequencies and two voltages in the large-signal regime.

A sensitivity study of the SW-TWT operation with respect to variations of other parameters, such as the radius of the beam tunnel and variation of the gap size has shown that a small interception current at a level of about 4 milliamps can be expected while the gain varies less than 10% from case to case.

Since the beam voltage is one of the experimentally controllable parameters, we completed a study on the SW-TWT operation for different voltages. The results of TESLA-SW/FW simulations for the as-built structure and the adjusted beam radius are presented in Fig. 4(a) and Fig. 4(b). The results of TESLA-SW/FW simulations presented in these figure show that the gain of the SW-TWT can be increased by 3 dB by variation of the beam voltage and the maximum output power can exceed 50 W. The predicted performance of the fabricated SW-TWT agrees well with the design goals of the 220 GHz SW-TWT [17].

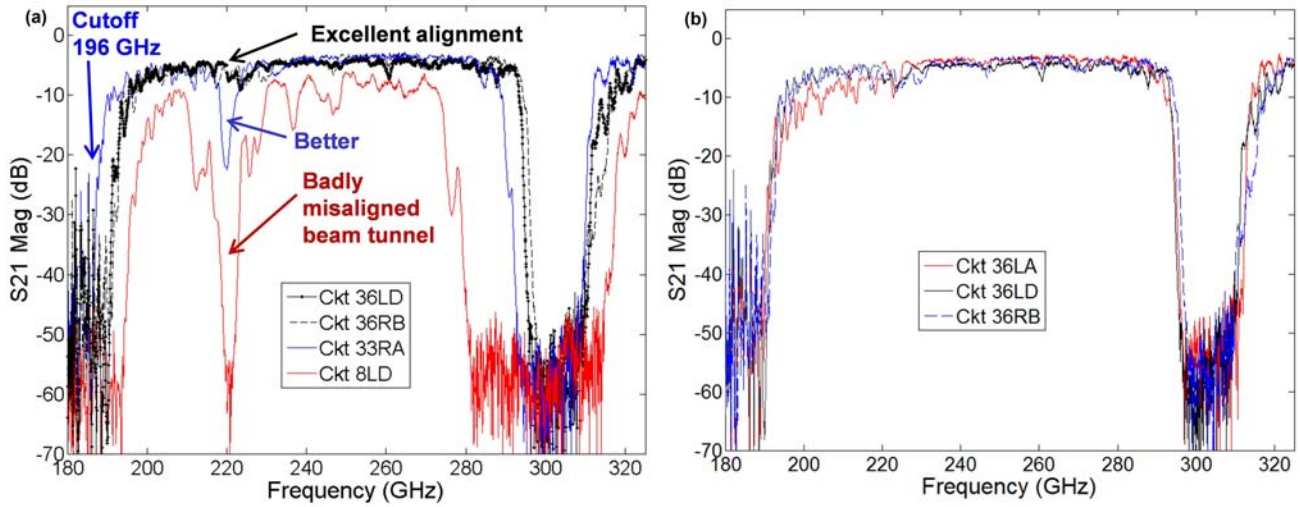

Figure 5. (a) Measurements of S_{21} transmission through several circuits comparing the effect of beam tunnel misalignment in the SW plane, which affects only the turn-to-turn phase uniformity, (b) VNA measurement of three circuits from the same wafer exhibiting astounding agreement in match of performance in S_{21}, indicating excellent tight tolerance control.

4. TESTING AND IMPROVING THE CIRCUITS

The cold test was done on an Agilent precision network analyzer (PNA) with Olson mmW extenders in the WR5 and WR3 waveguide sizes to inspect the response of the circuits from 140 GHz to 325 GHz.

4.1 Discovery of Beam Tunnel Alignment Effects

The first circuit cold tested was circuit #8LD, which exhibited a prominent stopband right at the $3\pi/2$ (270 deg) phase advance operating point at approximately 220 GHz (Fig. 5). After inspecting microscope measurements of the geometry, it was discovered that circuit #8LD had a slight tilt in the beam tunnel with respect to the SW plane (the x-direction of Fig. 1), which leads to a departure from the ideal mono-periodic phase advance from turn to turn, and into a quasi-periodic structure [18]. Several other early circuits exhibited either tilts or slight offsets in the beam tunnel with respect to the SW plane. A pure offset introduces a pure bi-periodicity and a strong stopband right around the $3\pi/2$ phase advance operating point, which is exactly between cutoff at the π-phase advance point and the upper stopband near the 2π-point. It should be noted that tilts or offsets in the depth-plane (the y-direction in Fig. 1) do not contribute to phase error, but only to beam-wave coupling and are not a significant source of frequency response ripple.

Several circuits that contain significant misalignment of the beam tunnel in the SW plane are compared in Fig. 5(a). The best circuits in the comparison were fabricated with special focus on improving beam tunnel alignment. Clearly, major reductions in the stopband severity at 220 GHz are possible with attention to alignment of this crucial feature. Theoretical estimates of the stopband width as a function of beam tunnel misalignment indicated that misalignments must be kept to under about 10% of the beam tunnel radius, or about 10 μm in this case, to keep the drop in power to less than 1.5 dB at the stopband center.

4.2 Corrective Action

In order to attempt to eliminate the stopband at the $3\pi/2$-pont, we focused on improving the alignment from layer-to-layer, as well as alignment of the beam tunnel filament to the first layer. Typical misalignment of the filament was under 10 microns (out of the beam tunnel radius of 95 microns) in the best circuits.

Some circuits in Fig. 5(a) exhibited greatly reduced stopbands, but were still found unacceptable due to residual misalignments between the two layers. Of the six circuits extracted from the latest wafer, three exhibited excellent S_{21} measurement results that are exceptionally well matched for this frequency range, resulting in an acceptable yield of 50%. Fig. 5(b) shows these truly remarkable measurements. Two of the circuits in particular measured so closely that they appear to be practically identical. All three circuits were located on different monofilaments of the same substrate, illustrating how accurately the filaments can be positioned. The measured beam tunnel misalignments in these circuits were in the range of 3 to 8 μm.

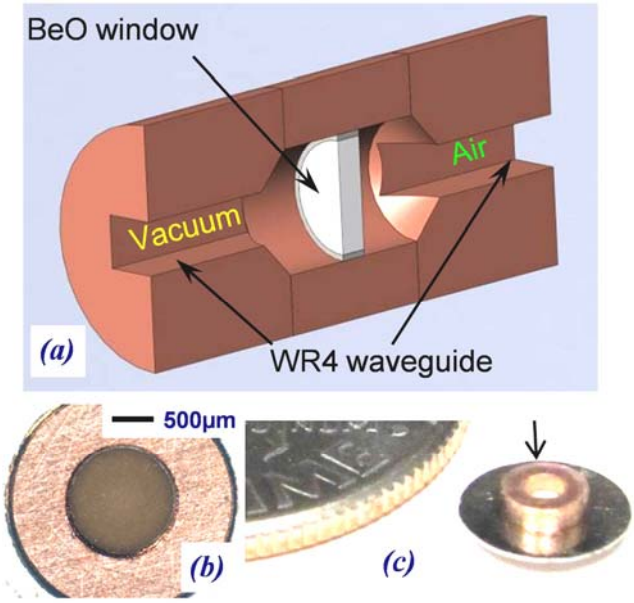

Figure 6: (a) Diagram of the pillbox window showing a tapered circular barrel region flanked by standard waveguide, (b) photo of beryllia window face, (c) window sub-assembly compared to a U.S. dime.

Other non-ideal features in the microfabrication contribute to stopbands as well, since any variation in a parameter that affects the phase from gap to gap can introduce a stopband if accumulated over enough periods. For example, slight non-uniformity in the thickness of the SU-8 layer can cause subtle distortions in the SU-8 mold which effectively alter the electromagnetic path lengths. Since these kinds of non-uniformities can be present over many periods, even a small distortion can add up to a measureable effect. Another issue is that SU-8 has a high thermal expansion coefficient and is known to delaminate itself or even crack over large surface areas [19]. During the fabrication process, this effect had been noted to manifest itself on the ends of the circuit that are connected to input and output waveguides by slightly pushing the first and last waveguide bends out of line by a few microns. Since it was a localized distortion, it did not appear to affect the performance of the circuits overall. Low temperature post-exposure baking has been suggested to mitigate internal stress in SU-8 [20].

5. WINDOW DESIGN AND TUNING

A pill-box resonant window design was selected to implement wide bandwidth vacuum windows [21]. Beryllia was chosen as the dielectric material due to difficulty in brazing diamond at such small sizes. Figure 6 shows the basic geometry of the vacuum window along with photographs of the window and sub-assembly. The window is brazed into a small cylindrical copper barrel and the resonance is tuned by lapping down the ends of the copper barrel until the S_{11} reflection drops to a minimum value. Figure 7 shows the measurement of the input and output windows after final tuning. At the -20 dB reflection level, the input and output windows exhibit about 23 GHz and 27 GHz bandwidth, respectively. The loss through the windows is negligible (<0.1 dB) over those bands. These windows had slightly different thicknesses to start with, so, when optimally tuned, their respective bands do not exactly overlap. This was intentional in order to prevent power from being reflected at the same frequency from both windows, avoiding the likelihood of a possible trapped-power resonance at a particular frequency. Since the gain profile is expected to have an extended high frequency tail, the passband of the windows is designed to be on the low end of the gain curve. In addition, the window stopband overlaps well with the stopband of the SW circuit at around 300 GHz, preventing trapped power near the 2π-phase advance operating point.

To ensure the windows were qualified for service at high power, the windows were tested at 2.5 W CW using the CPI, Inc. 218.4 GHz EIK amplifier, which is capable of 5 W output power. There were no incidents of arcing resulting from this test. The windows also passed a vacuum leak check.

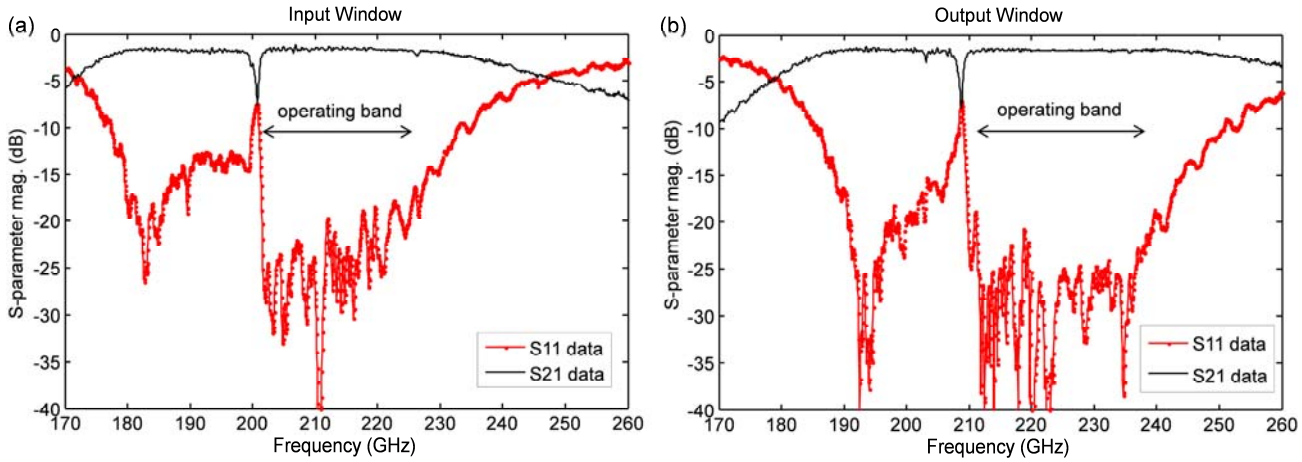

Figure 7: Measurements of (a) input window and (b) output window after final tuning. The frequency ranges are staggered on purpose to prevent power from being reflected at the same frequency, which could lead to oscillation. The measurements include losses of about 2 dB associated with the test fixture.

6. COMPLETED ASSEMBLY

Figure 8 shows a VNA measurement of the three best circuits mounted in the vacuum tube body with the windows installed. The circuits again exhibit excellent match in characteristics. Circuit #36LA was chosen for use in the tube because the others had minor defects in the circuits.

Circuit #36LA was successfully brazed into the copper body of the vacuum tube using a copper/silver foil alloy. The waveguides, window parts, and completed structure are show in Fig. 9, including a view of the 0.0075 inch diameter beam tunnel. Table II shows the final measured loss budget of the tube. Of the total cold loss of 6.6 dB, only 3.7 dB is attributable to the SW-TWT circuit, leaving 2.9 dB of unrecoverable waveguide losses. The tube body also passed vacuum leak checking and was sent to CPI, Inc. for integration with the electron gun, collector, and magnet system. The completed assembly is expected to begin hot testing at the end of calendar year 2012.

7. CONCLUSIONS

Ultraviolet photolithography shows great promise for microfabricating circuits in the upper-mmW and sub-mmW ranges through the THz. The enabling technique involved embedding UV-transparent monofilaments in the photoresist in order

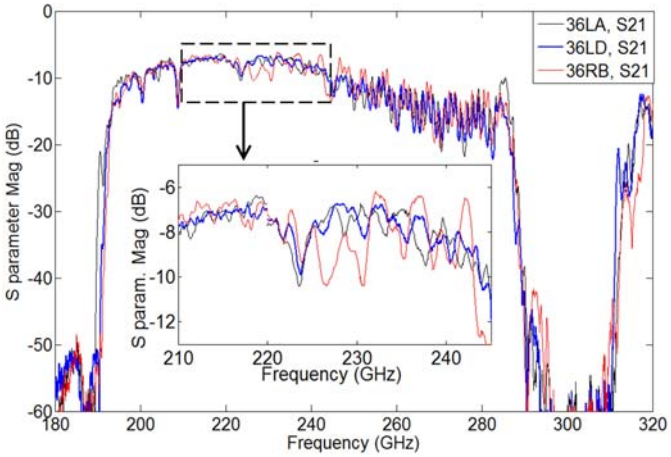

Figure 8: VNA measurement of three circuits from the same wafer exhibiting agreement in match of performance, indicating excellent tight tolerance control. There is a very small stopband of about 2 dB in magnitude at 224 GHz due to residual tolerance errors and beam tunnel misalignment.

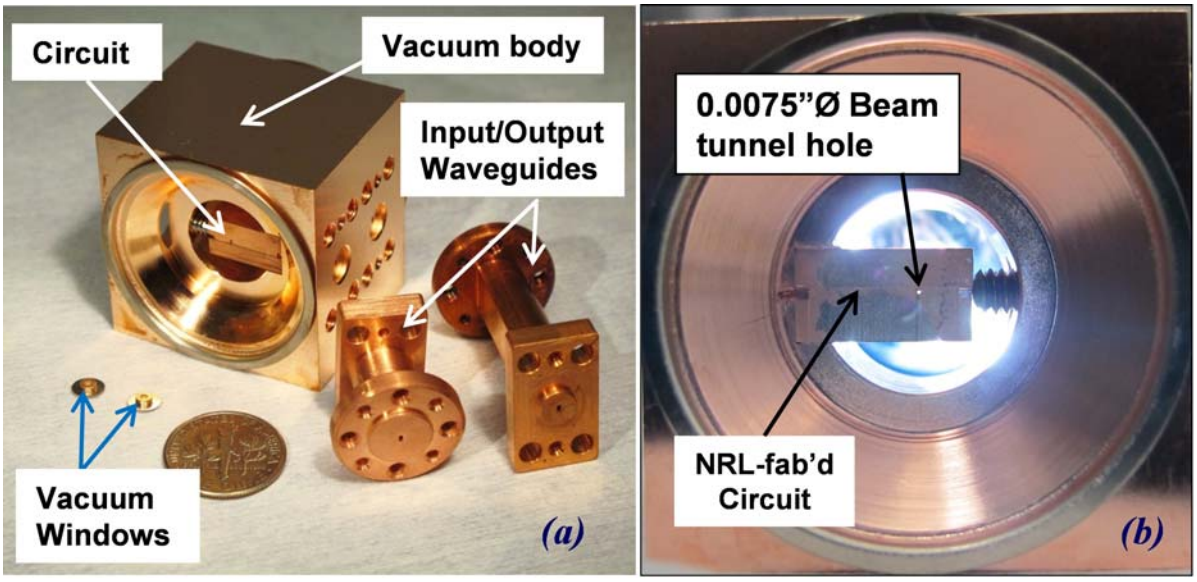

Figure 9: (a) Photographs of the completed circuit brazed into the vacuum body along with the windows, waveguides, and a U.S. dime (17.9 mm diameter); (b) Photograph of the brazed body assembly with beam tunnel hole visible.

Table 2. Loss Budget at 220 GHz.

Component	Measured Loss
WR4 90-deg E-plane bend	0.6 dB
Input waveguide (0.75 inch)	0.3
Input window loss	<0.1
Body input taper	0.4
On-circuit input taper	0.3
Serpentine Waveguide circuit	3.7
On-circuit output taper	0.3
Body output taper	0.4
Output window loss	<0.1
Output waveguide (1.5 inch)	0.6
Total Cold Loss	**6.6 dB**
Total waveguide losses	**2.9 dB**

to hold the shape of the electron beam tunnels while precise optical techniques form the molds needed for electroforming. At present, we have succeeded in applying these techniques at 670 GHz and are quickly moving toward THz fabrication while demonstrating the viability of the technique at 220 GHz in a working prototype vacuum tube.

During the cold testing phase of the program, it was discovered that even slight misalignments of the beam tunnel cause large stopbands to open up, making the amplifier highly susceptible to oscillations. By very careful alignment of the monofilaments, the beam tunnels were aligned well enough to prevent major problems with oscillations.

8. ACKNOWLEDGEMENT

This work was sponsored in part by DARPA and by the U.S. Office of Naval Research. The authors wish to acknowledge the work of Mr. R. E. Myers for brazing the circuits, Mr. B. S. Albright Jr. for highly precise EDM, and Mr. F. N. Wood for fabricating the lithography masks.

REFERENCES

[1] Booske, J. H., Dobbs, R. J., Joye, C. D., Kory, C. L., Neil, G. R., Park, G. S., Park, J. H., Temkin, R. J., "Vacuum electronic high power terahertz sources," *Trans. THz Science and Technology* **1**(1) 54-75 (2011).

[2] Del Campo, A., Greiner, C., "SU-8: A photoresist for high-aspect-ratio and 3D photolithography," *J. Micromech./ Microeng.,* 17, R81-R95, (2007).

[3] Joye, C. D., Calame, J. P., Garven, M., Levush, B., "UV-LIGA microfabrication of 220 GHz sheet beam amplifier gratings with SU-8 photoresist," *J. Micromech. / Microeng,* 20, 125016 (2010).

[4] So, J. K., Shin, Y. M., Jang, K. H., Won, J. H., Srivastava, A., Sattorov, M. A., Park, G. S., Kim, J. H., Chang, S. S., "Experimental study on 100 GHz two-step LIGA-based backward wave devices," *8th Int'l Vac. Elec. Conf. (IVEC)*, Kitakyushu, Japan, 369-370 (2007).

[5] Shin, Y.-M., Barnett, L. R., Luhmann, N. C. Jr., "MEMS-fabricated micro vacuum electron devices (μVEDs) for terahertz (THz) applications," *Proc. IRMMW-THz Conf., Pasadena, CA,* T4K1.1591 (2008).

[6] Tucek, J. C., Basten, M. A., Gallagher, D. A., Kreischer, K. E., "220 GHz Power Amplifier Development at Northrop Grumman," Conf. Proc., IVEC-IVESC, Monterey, CA (2012).

[7] Tucek, J. C., Basten, M. A., Gallagher, D. A., Kreischer, K. E., Lai, R., Radisic, V., Leong, K., Mihailovich R., "A 100 mW, 0.670 THz Power Module," Conf. Proc., IVEC-IVESC, Monterey, CA (2012).

[8] Basten, M. A., Tucek, J. C., Gallagher D. A., Kreischer, K. E., Mihailovich, R., "A 0.85 THz Vacuum-Based Power Amplifier," Conf. Proc., IVEC-IVESC, Monterey, CA (2012).

[9] Joye, C. D., Calame, J. P., Nguyen, K. T., Garven, M., "Microfabrication of Fine Electron Beam Tunnels using UV-LIGA and Embedded Polymer Monofilaments for Vacuum Electron Devices," *J. Micromech. / Microeng.*, 22(1) 015010 (2012).

[10] U.S. Patent Application No. 13/420,696 (March 15, 2012); Foreign PCT Patent Application No. 61/471,828. Inventor: Joye, C. D.

[11] Steer, B., Hyttinen, M., Roitman, A., Horoyski, P., Smith, G. M., Bolton, D. R., Cruickshank, P. A. S., Robertson, D. A., "Compact, high power EIK sources used for ESR and NMR," *33rd Int'l Conf on Infrared, Millimeter and Terahertz Waves (IRMMW-THz)*, (2008).

[12] Vlasov, A. N., Antonsen, T. M. Jr., Chernyavskiy, I. A., Chernin, D. P., Levush, B., "A Computationally Efficient Two Dimensional Model of the Beam-Wave Interaction in a Coupled Cavity TWT," *IEEE Trans. Plasma Science*, 40(6) 1575-1589 (2012).

[13] Antonsen, T. M. Jr., Chernin, D., Vlasov, A., Chernyavskiy, I., Levush, B., Nguyen, K., "A simple hybrid model for folded waveguide structures," *Book of abstracts, IVEC-IVESC*, Monterey, CA (2012).

[14] Chernyavskiy, I. A., Vlasov, A. N., Levush, B., Antonsen, T. M. Jr, "2D modeling of TWTs based on serpentine and folded waveguide structures," *Book of abstracts, ICOPS*, Edinburgh, UK (2012).

[15] ANALYST™ electromagnetic solver, AWR Corp., El Segundo, CA, 2012.

[16] Petillo, J., et al., "The MICHELLE Three-Dimensional Electron and Collector Modeling Tool: Theory and Design", *IEEE Trans. Plasma Sci.*, 30(3) 1238-1264 (2002).

[17] Nguyen, K. T., Pasour, J., Wright, E., Abe, D. K., Ludeking, L., Pershing, D., Levush, B. "Linearity performance of multi-stage TWT amplifiers: cascade vs. series," *12th Int'l Vac. Elec. Conf. (IVEC),* Bangalore, India, 309-310 (2011).

[18] Cook, A. M., Joye, C. D., Calame, J. P., Nguyen, K. T., Vlasov, A., Wright, E. L., Abe, D. K., Levush, B., "Serpentine waveguide 220 GHz millimeter wave amplifier cold test," 13th *Int'l Vac. Elec. Conf. (IVEC),* 547-548 (2012).

[19] Lin, C.-H., Lee, G.-B., Chang, B.-W., Chang, G.-L., "A new fabrication process for ultra-thick microfluidic microstructures utilizing SU-8 photoresist," *J. Micromech./Microeng.*, 12, 590-597 (2002).

[20] Li, B., Liu, M., Chen, Q., "Low-stress ultra-thick SU-8 UV photolithography process for MEMS," *J. Microlith., Microfab., Microsyst.*, 4(4) 043008 (2005).

[21] Cook, A. M., Joye, C. D., Kimura, T., Wright, E. L., Calame, J. P., "Broadband 220 GHz Vacuum Window for a Traveling Wave Tube Amplifier," *Submitted to IEEE J. Trans. Electron Dev.*, Sept. 2012.